# Global Phosphoproteome Profiling Reveals Unanticipated Networks Responsive to Cisplatin Treatment of Embryonic Stem Cells[▽][†]

Alex Pines,[1] Christian D. Kelstrup,[2] Mischa G. Vrouwe,[1]‡ Jordi C. Puigvert,[3]‡ Dimitris Typas,[1]‡
Branislav Misovic,[1] Anton de Groot,[1] Louise von Stechow,[3] Bob van de Water,[3]
Erik H. J. Danen,[3] Harry Vrieling,[1]* Leon H. F. Mullenders,[1]*
and Jesper V. Olsen[2]

*Department of Toxicogenetics, Leiden University Medical Center, P.O. Box 9600, 2300 RC Leiden, The Netherlands[1]; Department of Proteomics, Novo Nordisk Foundation Center for Protein Research, Faculty of Health Sciences, University of Copenhagen, Blegdamsvej 3b, 2200 Copenhagen N, Denmark[2]; and Division of Toxicology, Leiden/Amsterdam Center for Drug Research, Leiden University, P.O. Box 9502, 2300 RA Leiden, The Netherlands[3]*

Cellular responses to DNA-damaging agents involve the activation of various DNA damage signaling and transduction pathways. Using quantitative and high-resolution tandem mass spectrometry, we determined global changes in protein level and phosphorylation site profiles following treatment of SILAC (stable isotope labeling by amino acids in cell culture)-labeled murine embryonic stem cells with the anticancer drug cisplatin. Network and pathway analyses indicated that processes related to the DNA damage response and cytoskeleton organization were significantly affected. Although the ATM (ataxia telangiectasia mutated) and ATR (ATM and Rad3-related) consensus sequence (S/T-Q motif) was significantly overrepresented among hyperphosphorylated peptides, about half of the >2-fold-upregulated phosphorylation sites based on the consensus sequence were not direct substrates of ATM and ATR. Eleven protein kinases mainly belonging to the mitogen-activated protein kinase (MAPK) family were identified as being regulated in their kinase domain activation loop. The biological importance of three of these kinases (cyclin-dependent kinase 7 [CDK7], Plk1, and KPCD1) in the protection against cisplatin-induced cytotoxicity was demonstrated by small interfering RNA (siRNA)-mediated knockdown. Our results indicate that the cellular response to cisplatin involves a variety of kinases and phosphatases not only acting in the nucleus but also regulating cytoplasmic targets, resulting in extensive cytoskeletal rearrangements. Integration of transcriptomic and proteomic data revealed a poor correlation between changes in the relative levels of transcripts and their corresponding proteins, but a large overlap in affected pathways at the levels of mRNA, protein, and phosphoprotein. This study provides an integrated view of pathways activated by genotoxic stress and deciphers kinases that play a pivotal role in regulating cellular processes other than the DNA damage response.

Cancer chemotherapy drugs are designed to selectively kill cells that divide rapidly, which is a main feature of most cancer cells. Cisplatin [*cis*-diamminedichloroplatinum(II); CDDP] is among the most widely employed drugs in chemotherapy administered as a curative treatment for several forms of cancer, including ovarian, cervical, head and neck, esophageal, non-small-cell lung, and, especially, testicular cancer (23, 26, 32). Cisplatin binds to DNA and forms a spectrum of intra- and interstrand DNA cross-links as well as mono adducts. These DNA adducts are thought to mediate their cytotoxic effects by interfering with transcription and replication, ultimately leading to the induction of apoptosis (62). Cisplatin adducts distort the DNA duplex, resulting in the exposure of the DNA minor groove, to which

several classes of proteins can bind, including high-mobility group (HMG) proteins and transcription factors that contribute to cisplatin-induced toxicity (70).

Repair of cisplatin-DNA adducts involves proteins from multiple DNA repair pathways: i.e., nucleotide excision repair (NER), homologous recombination, postreplication repair, and mismatch repair (MMR) (11, 70). NER is the major pathway responsible for the removal of cisplatin-DNA adducts *in vitro* and *in vivo* (15, 69), and hence, the marked sensitivity of testicular cancer to cisplatin has been correlated with low levels of NER proteins, i.e., XPA and ERCC1-XPF (74). DNA damage caused by cisplatin activates several signal transduction pathways, including mitogen-activated protein kinase (MAPK), AKT, c-ABL, and ATM (ataxia telangiectasia mutated)/ATR (ATM and Rad3-related)/DNA-protein kinase (PK)-dependent pathways regulating a variety of processes, such as drug uptake, DNA damage signaling, cell cycle arrest, DNA repair, and cell death (70).

Treatment of patients with cisplatin is compromised by the substantial risk of severe toxicity—i.e., anemia, nausea, and neurotoxicity (31). Tumors frequently become resistant to the drug (4, 37), and multiple resistance mechanisms have been identified, including increased cellular efflux or decreased cel-

lular import of cisplatin (16, 53). Cisplatin resistance can also occur through enhanced DNA damage repair or increased tolerance to DNA damage (4).

Improvement of cancer therapy mediated by chemotherapeutic drug agents such as cisplatin requires better understanding of the cellular pathways underlying toxicity and drug resistance. Indeed, most of the recent advances in cancer treatment are based on drastic improvements in conceptual understanding of cellular networks. Cellular responses to DNA damage such as cisplatin-induced intra- and interstrand DNA crosslinks are controlled by a global signaling network called the DNA damage response (DDR) (17) and mediated by posttranslational protein modifications (6). One of the most frequent modifications is the reversible and dynamic phosphorylation of proteins at specific serine, threonine, and tyrosine residues that control the activity of the majority of cellular processes. It has been estimated that almost 70% of all proteins in mammalian cells are phosphorylated at some point during their expression (42). Key signaling molecules in DDR are the protein kinases ATM (ataxia telangiectasia mutated) and ATR (ATM and Rad3-related) (1). Matsuoka and coworkers recently identified over 900 phosphorylation sites in about 700 proteins by phosphoproteome analysis of proteins targeted by the ATM and ATR kinases after exposure to ionizing radiation (30); however, knowledge of the genomewide protein phosphorylation response to genotoxic insults is still limited. This study aimed to identify the molecular processes and cellular pathways that are affected after treatment with cisplatin, one of the most commonly used chemotherapeutic drugs. To achieve these goals, we examined the cisplatin-induced stress responses, changes in protein level, and global phosphorylation site profiles by quantitative phosphoproteomics. Besides activation of the DDR kinases ATM and ATR, we identified 11 other protein kinases with altered activities in response to cisplatin. We applied small interfering RNA (siRNA)-mediated knockdown to demonstrate that 3 kinases have important protective roles in the cellular response to cisplatin-induced toxicity. Our data set identified the cytoskeleton as a novel target of the cisplatin-induced stress response. In addition, integration of transcriptome, proteome, and phosphoproteome data disclosed a strong correlation in the affected pathways at the levels of transcription and protein phosphorylation.

## MATERIALS AND METHODS

**Cell culture and cisplatin treatment.** Cell culture and cisplatin treatment of wild-type mouse embryonic stem (mES) cells (B4418 and HM1 derived from the C57/Bl6 and OLA/129 mouse genetic backgrounds, respectively) were essentially performed as previously described (24). Subconfluent cultures of mES cells were exposed to cisplatin (5 μM) added directly to the culture medium. Cell cultures were incubated for different periods after cisplatin administration (0.5, 2, 4, and 8 h). The Thermo Scientific Pierce mouse embryonic stem cell kit, containing media and reagents specifically designed for analysis of protein by mass spectrometry (Thermo Scientific), was used for SILAC (stable isotope labeling by amino acids in cell culture) experiments.

**Phosphopeptide enrichment.** Isolation and purification of phosphopeptides were performed according to already published procedures (68), with some modifications. Briefly, cells were lysed for 30 min in lysis buffer (8 M urea, 50 mM Tris [pH 8.1], 75 mM NaCl, 1 mM MgCl₂, 500 U benzonase and phosphatase inhibitors). Samples were centrifuged for 15 min at 13,000 rpm, and the protein concentration was established by Qubit protein assay (Invitrogen). Ten milligrams of proteins was first reduced with 2.5 mM dithiothreitol (DTT) for 25 min

at 60°C and subsequently alkylated by incubation with 7 mM iodoacetamide for 15 min at room temperature, protected from light. The alkylation reaction was quenched by incubation with 2.5 mM DTT for 15 min at room temperature. Protein solution was diluted 8-fold with 25 mM Tris (pH 8.1)–1 mM CaCl₂ and incubated for 15 h at 37°C with 100 μg trypsin (Promega). On the following day, the digestion reaction was stopped by addition of trifluoroacetic acid (TFA) to a 0.4% final concentration, and the precipitate was removed by centrifugation for 5 min at 3,200 rpm. The supernatant was loaded on a Sep-Pak Vac 1-ml C₁₈ cartridge (Waters), desalted by washing with 0.1% acetic acid, and eluted with 0.1% acetic acid–30% acetonitrile. Eluted peptides were lyophilized and fractionated at 1 ml/min on a 9.4- by 200-mm 5-μm-particle polysulfoethyl A strong cation exchange (SCX) column (PolyLC) using a 70-min gradient from 0 to 75 mM KCl, with 350 mM KCl for 38 min in 5 mM KH₂PO₄ (pH 2.65), and 30% acetonitrile. Eighteen fractions with 6 ml eluate were collected, desalted on a Sep-Pak Vac 1-ml C₁₈ cartridge, and lyophilized as described above before. In the desalting step, the last eight fractions were reduced to four fractions by loading two fractions on one cartridge, giving a total of 14 fractions. After lyophilization, peptides were dissolved in solution A (300 mg/ml lactic acid, 80% acetonitrile, 0.1% TFA) and loaded on a titanium tip column (TopTip 1 −100 μl; Glycen Corporation) prewashed with elution solution (15 mM NH₄OH, pH~10.5), equilibration solution (0.1% TFA), and solution A. After sample loading, the tip column was washed with solution A and B (80% acetonitrile [vol/vol], 0.1% TFA [vol/vol]). After washing, phosphopeptides were eluted with elution buffer and collected in an equal volume of 2% TFA. For desalting, phosphopeptides were loaded on a Stage Tip C₁₈ column (Proxeon) prewashed with methanol, solution B, and 0.1% TFA. The phosphopeptide solution was loaded on a Stage Tip column, washed with 0.1% TFA, and eluted with solution B. Liquid was removed by lyophilization and stored at −80°C until mass spectrometry (MS) analysis.

**Mass spectrometric analysis. (i) LC-MS/MS.** The dried phosphopeptide mixtures were acidified with 5% acetonitrile in 0.3% trifluoroacetic acid (TFA) to an end volume of 10 μl, transferred to a 96-well plate, and analyzed by online nanoflow liquid chromatography-tandem mass spectrometry (nano-LC-MS/MS) as described previously (41) with a few modifications. Briefly, all nano-LC-MS/MS-experiments were performed on an EASY-nLC system (Proxeon Biosystems, Odense, Denmark) connected to the LTQ-Orbitrap Velos (Thermo Electron, Bremen, Germany) through a nanoelectrospray ion source.

Five microliters of each phosphopeptide fraction was autosampled onto and directly separated in a 15-cm analytical column (75-μm inner diameter) packed in-house with 3-μm C₁₈ beads (Reprosil-AQ Pur, Dr. Maisch) with a 90-min gradient from 5% to 30% acetonitrile in 0.5% acetic acid at a flow rate of 250 nl/min. The effluent from the high-performance liquid chromatography (HPLC) was directly electrosprayed into the mass spectrometer by a platinum-based liquid junction.

The LTQ-Orbitrap Velos instrument was operated in the data-dependent mode to automatically switch between full-scan MS and MS/MS acquisition. Instrument control was through Tune 2.6.0, and Xcalibur 2.1 Survey full-scan MS spectra (from m/z 300 to 2,000) were analyzed in the Orbitrap detector with resolution of 30,000 at m/z 400 (after accumulation to a "target value" of 1e6 in the linear ion trap). The 10 most intense peptide ions with charge states of ≥2 were sequentially isolated to a target value of 5e4 and fragmented in an octopole collision cell by higher-energy collisional dissociation (HCD) with a normalized collision energy setting of 40%. The resulting fragments were detected in the Orbitrap system with resolution of 7,500. The ion selection threshold was 5,000 counts, and the maximum allowed ion accumulation times were 500 ms for full scans and 250 ms for HCD.

Standard mass spectrometric conditions for all experiments were as follows: spray voltage, 2.2 kV; no sheath and auxiliary gas flow; heated capillary temperature, 275°C; predictive automatic gain control (pAGC) enabled, and an S-lens RF level of 65%. For all full-scan measurements with the Orbitrap detector, a lock mass ion from ambient air (m/z 445.120024) was used as an internal calibrant as described previously (39). A setting was also chosen where the additional single injection method (SIM) injection of the lock mass is deactivated, in order to save time.

**(ii) Raw MS data analysis: peptide identification and quantitation by MASCOT and MaxQuant.** Raw Orbitrap full-scan MS and ion trap MSA spectra were processed by MaxQuant as described previously (7, 8). In brief, all identified SILAC doublets were quantified, accurate precursor masses were determined based on intensity-weighing precursor masses over the entire LC elution profiles, and MS/MS spectra were merged into peak-list files (*.msm). Peptides and proteins were identified by Mascot (Matrix Science, London, United Kingdom) via automated database matching of all tandem mass spectra against an in-house curated concatenated target/decoy database; a forward and reversed version of

the mouse International Protein Index (IPI) sequence database (version 3.37; 102,934 forward and reversed protein sequences from EBI [http://www.ebi.ac.uk /IPI/]) supplemented with common contaminants such as human keratins, bovine serum proteins, and porcine trypsin. Tandem mass spectra were initially matched with a mass tolerance of 7 ppm on precursor masses and 0.02 Da for HCD fragment ions. Scoring was performed in MaxQuant as described previously. We required strict trypsin enzyme specificity and allowed for up to two missed cleavage sites. Cysteine carbamidomethylation (Cys, +57.021464 Da) was searched as a fixed modification, whereas N-acetylation of proteins (N-terminal, +42.010565 Da), N-pyroglutamine (−17.026549 Da), oxidized methionine (+15.994915 Da), and phosphorylation of serine, threonine, and tyrosine (Ser/Thr/Tyr, +79.966331 Da) were searched as variable modifications.

**Peptide filtering and phosphorylation site localization.** The resulting Mascot result files (*.dat) were loaded into the MaxQuant software suite for further processing. In MaxQuant, we fixed the estimated false discovery rate (FDR) of all peptide and protein identifications at 1%, by automatically filtering on peptide length, mass error precision estimates, and the Mascot score of all forward and reversed peptide identifications. Finally, to pinpoint the actual phosphorylated amino acid residue(s) within all identified phosphopeptide sequences in an unbiased manner, MaxQuant calculated the localization probabilities of all putative serine, threonine, and tyrosine phosphorylation sites, using the PTM score algorithm as described previously (38).

**Phosphorylation site sequence motif logo plots.** Only peptides with localization probabilities of >0.75 were included in the downstream bioinformatic analysis (see Table S1 in the supplemental material). To identify enriched sequence motifs in the phosphorylation site data set, we made use of the already published kinase motifs (www.phosida.com) and an algorithm that extracts overrepresented motifs in a more unbiased manner (58). The algorithm was implemented in R (a programming language and software environment for statistical computing and graphics), using a Fisher's exact test to iteratively test for position-specific overrepresentation of amino acid groups between two lists of prealigned sequences. The perl-package WebLogo was used internally in the algorithm to visualize the enriched sequence motifs as logo plots. Grouping of amino acids was done on the basis of related chemical properties (acidic, basic, aromatic, aliphatic, hydrophilic, amide, polar, and cyclic), and alignment was done with a sequence window of ±6 amino acids surrounding the central phosphorylated serine, threonine, or tyrosine residue. The iterative nature of the algorithm means it is successively reapplied on the result from an analysis—i.e., on both the subset of the lists which contains the most significantly overrepresented amino acid group and the subset that does not contain this amino acid group. All cisplatin-regulated phosphorylation site sequences were compared to all unchanging sites and vice versa. We considered a motif significant if it fulfilled our conservative cutoff of $P < 0.001$ on the Bonferroni adjusted $P$ values.

**Network and pathway analyses.** Network and pathway analyses were performed using MetaCore software (http://www.genego.com/metacore.php). Proteins containing upregulated phosphorylation sites (>1.5-fold and >2-fold) and downregulated phosphorylation sites (>1.5-fold and >2-fold) were investigated. In most cases, high-throughput experiments result in lists of genes or proteins of interest. The data sets usually contain anywhere between a few dozen and few thousand genes/proteins. In MetaCore, the significance is evaluated based on the size of the intersection between the user's data set and set of genes/proteins corresponding to a network module/pathway in question, or rather the probability to randomly obtain an intersection of a certain size between the user's set and a network/pathway follows a hypergeometric distribution. The significance of the networks/pathways is evaluated for whether the algorithm has succeeded in creating modules that have a higher-than-random saturation with the genes of interest.

Networks are drawn from scratch by GeneGo annotators and manually curated and edited. There are about 110 cellular and molecular processes whose contents have been defined and annotated by GeneGo. Canonical pathway maps represent a set of about 650 signaling and metabolic maps covering human biology (signaling and metabolism) in a comprehensive way.

**Western blot analysis.** Total cell extracts were obtained by direct lysis of the cells in Laemmli-SDS-sample buffer. Western blot analysis was performed as described previously (13), and protein bands were analyzed and visualized with the Odyssey infrared imaging system (LI-COR) using secondary antibodies labeled with visible fluorophores. The antibodies employed were mouse anti-γ-H2AX (Millipore), rabbit anti-H2B (Santa-Cruz), mouse anti-p53 (Santa Cruz Biotechnology DO-1), rabbit anti-cyclin-dependent kinase 7 (anti-CDK7; Cell Signaling), rabbit anti-PLK1 (Cell Signaling), rabbit anti-KPCD1 (Cell Signaling), rabbit anticentrin (Cell Signaling), rabbit anti-E-cadherin (Cell Signaling), and rabbit anti-mark2 (Cell Signaling).

**Flow cytometry analysis.** For cell cycle analysis, samples were either treated with 5 μM cisplatin for 0.5, 2, 4, or 8 h or mock treated, after which 5-ethynyl-2′-deoxyuridine (EdU) label was added to a final concentration of 20 μM. Cells were collected 45 min after addition of EdU label and stained for EdU and DNA using the Click-iT EdU flow cytometry assay kit (Invitrogen) according to the manufacturer's protocol.

To determine the mitotic index, samples were either treated with 5 μM cisplatin for 0.5, 2, 4, or 8 h, treated with 100 ng/ml nocodazole for 4 h, or mock treated. Cells were collected and $10^6$ cells were fixed with 70% ethanol. Cells were washed with phosphate-buffered saline (PBS) and incubated with rabbit anti-phospho-Ser10 histone H3 antibody (Millipore). After washing, samples were incubated with goat anti-rabbit antibody–Alexa Fluor 488 (Invitrogen). After washing, cells were treated with RNase A (200 μg/ml) and stained with propidium iodide (Bio-Rad). Cells were analyzed using a BD LSR II flow cytometer (BD Biosciences) and FACSDiva 5.0 software. Results were analyzed with WinMDI 2.8 software.

**Immunofluorescence staining.** Cells were fixed in 4% formaldehyde in CSK buffer, consisting of 100 mM NaCl, 300 mM sucrose, 10 mM PIPES [piperazine-N,N′-bis(2-ethanesulfonic acid); pH 6.8],and 3 mM MgCl2, and permeabilized by treatment with 0.5% Triton X-100 in PBS for 10 min. Actin was visualized by DY554-phalloidin (Sigma-Aldrich), and cells were counterstained with DAPI. Images were captured with a Zeiss Axioplan2 microscope equipped with a Zeiss Axiocam MRm camera using either a Plan-NEOFLUAR 40×/1.30 or 63×/1.25 objective.

**siRNA transfection.** HM1 mES cells were transfected with a 50 nM final concentration of siRNA (Dharmacon), targeting for CHK2, CDK7, MAPK2, M3K2, MK14, MARK1, PDPK1, PLK1, KPC1, KPCD1, and SG269, as well as siRNA coding for green fluorescent protein (siGFP; control 1) and siRNA coding for LAMIN A/C (siLAMIN A/C; control 2), which were used as negative controls. Transfection was performed using Dharmafect 1 (Dharmacon) according to the manufacturer's instructions. A total of $10^3$ HM1 mES cells were transfected for 16 h in μClear 96-well plates (Greiner), and the medium was refreshed every 24 h for 48 h.

**Cell viability assay.** At 64 h post-siRNA transfection, HM1 mES cells were treated with either vehicle or 10 μM cisplatin (Ebewe Pharma) for 24 h. ATP Lite (Perkin Elmer) was then used for the assessment of cell viability according to the manufacturer's instructions. As an additional confirmation that cisplatin was inducing apoptosis, the pan-caspase inhibitor benzyloxycarbonyl-Val-Ala-DL-Asp(OMe)-fluoromethylketone (zVAD-fmk) (Bachem, Bubendorf, Switzerland) was used to inhibit caspases and block cisplatin-induced apoptosis (see Fig. S4A in the supplemental material).

**Gene expression analysis.** The gene expression levels of Cdh1, p53, centrin2, and mark2 were quantified after exposure to 5 μM cisplatin for 4 h using quantitative reverse transcriptase-PCR (qRT-PCR). The qRT-PCR was performed using the Applied 7900ht real-time PCR detection system (Applied Biosystems). In three independent experiments, the RNA was isolated from mES cells and purified using an RNeasy kit (Qiagen). qRT-PCR was performed using the FastStart Universal SYBR green master (Rox) (Roche) according to the manufacturer's instructions.

The following primers were used: Cdh1 forward (ATCCTCGCCCTGCTGATT) and reverse (ACCACCGTTCTCCTCCGTA), p53 forward (ATGCCCATGCTACAGAGGAG) and reverse (AGACTGGCCCTTCTTGGTCT), centrin2 forward (TGAGACTGGGAAAATATCATTCAA) and reverse (CACCATCTCCATCTCGATCA), and mark2 forward (GAAAGGGACACGGAGCAG) and reverse (CCGCAGCATGTTGGACTT).

mRNA expression values were normalized to the housekeeping gene coding for hypoxanthine guanine phosphoribosyltransferase (HPRT).

# RESULTS

**Cisplatin-induced stress responses.** Murine embryonic stem (mES) cells were selected as the cellular model for this study since they have the unique combination of a virtually infinite life span with uncompromised DDR. mES cells manage to maintain their genomic integrity through robust defense mechanisms against DNA damage, including effective DNA repair and a hypersensitive apoptotic response (61). These characteristics make mES cells suitable to study the molecular events that underlie the cellular responses related to cisplatin-induced toxicity. To assess the kinetics of the cisplatin-induced stress
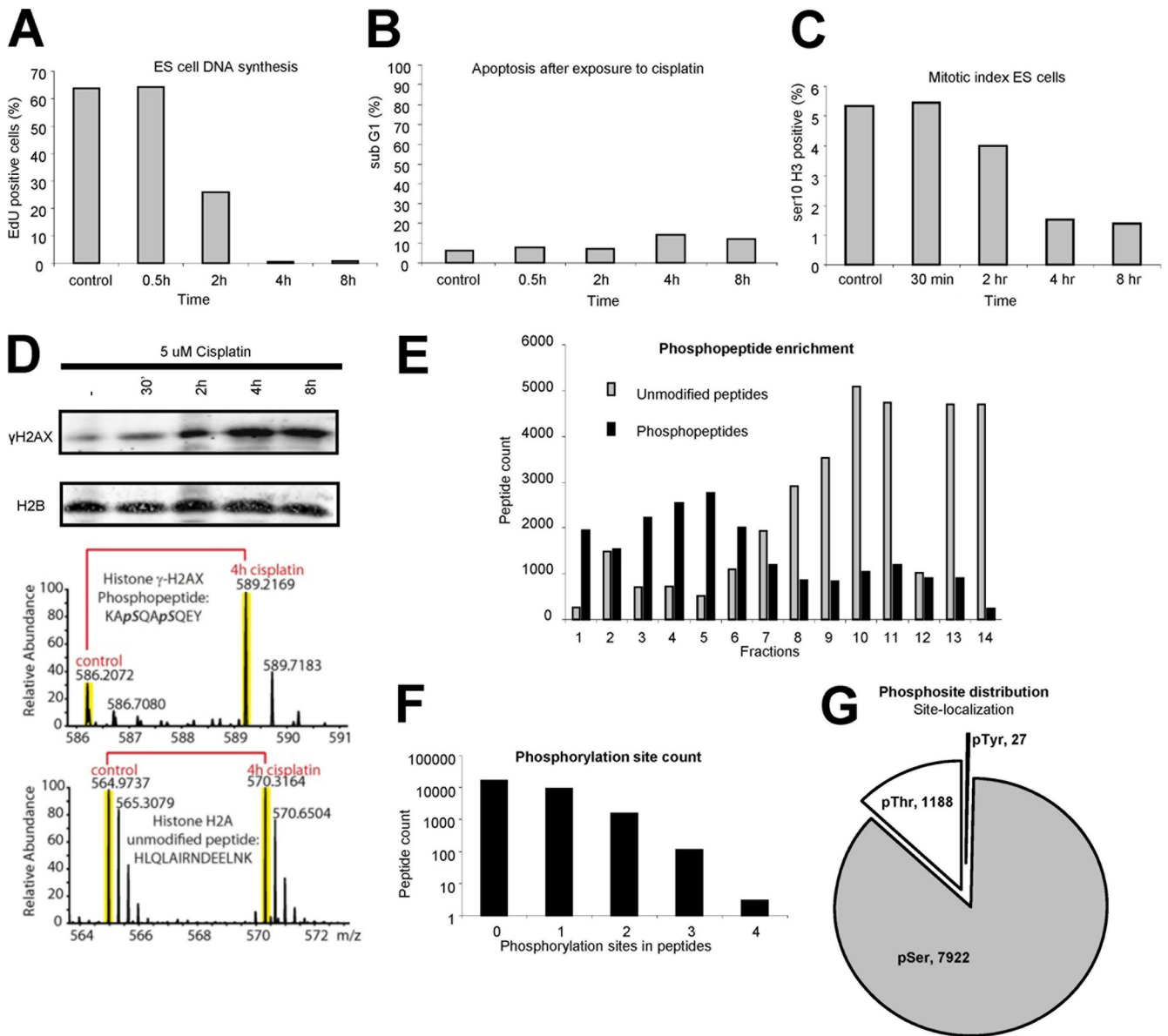
FIG. 1. (A) mES cells were treated with 5 μM cisplatin for different times (as indicated) followed by EdU labeling for 45 min. Flow cytometric analysis evidenced a time-dependent inhibition of DNA synthesis. (B) mES cells were treated with 5 μM cisplatin, and the sub-$G_1$ cell content was determined by flow cytometric analysis at different time points (as indicated). (C) The mitotic index of mES cells treated with 5 μM cisplatin was determined at different time points (as indicated) by flow cytometric analysis. (D) mES cells were treated with 5 μM cisplatin and analyzed 0.5, 2, 4, and 8 h later with the indicated antibodies. −, untreated sample. Shown are the SILAC mass spectrometry spectra of γ-H2AX phosphopeptide and unmodified H2A peptide. (E) Number of phosphopeptides (black bars) and unmodified peptides (gray bars) identified by MS analysis. (F) Number of peptides containing 0, 1, 2, 3, and 4 phosphorylation sites. (G) Phosphorylation site distribution over serine, threonine, and tyrosine residues.

response, we examined cell cycle progression, mitotic index, and DNA strand breaks (by staining for γ-H2AX) in cisplatin-exposed mES cells over time. Cell cycle analysis following DNA synthesis labeling by EdU showed that, in the absence of cisplatin, about 65% of the ES cells were in S phase ($G_1$, ~15%; and $G_2$/M, ~20%; see Fig. S1A in the supplemental material). After addition of cisplatin, we observed a time-dependent inhibition of DNA synthesis: the incorporation of EdU was evident at 30 min, decreased after 2 h, and was completely absent at 4 and 8 h (Fig. 1A). Inhibition of DNA

replication and transcription has been widely considered to be a key to the mechanism of cisplatin cytotoxicity (62). No significant induction of apoptosis (estimated from the sub-$G_1$ content) occurred during the treatment period (Fig. 1B), in agreement with previous results (24). In the absence of cisplatin, about 5% of the cells were in mitosis, as estimated by fluorescence-activated cell sorter (FACS) analysis of serine 10 phosphorylation of histone H3; nocodazole-treated cells arrested in $G_2$ or M phase were used as a positive control (see Fig. S1B in the supplemental material). The maximal reduction

in mitotic index was observed after 4 h of cisplatin treatment and persisted through 8 h (Fig. 1C). Cisplatin-mediated DNA damage signaling manifested by γ-H2AX phosphorylation increased with time, reaching its maximal level at 4 h posttreatment, as evidenced by Western blotting and MS analysis (Fig. 1D). Together, these time course experiments indicated a complete inhibition of DNA synthesis, a significant reduction of mitotic index, and a strong induction of DNA damage signaling after 4 h of cisplatin treatment.

**Phosphoproteome analysis after cisplatin exposure.** Stable isotope labeling by amino acids in cell culture (SILAC) technology (43) was applied to quantitatively and qualitatively analyze genomewide protein phosphorylation events following exposure to cisplatin. mES cells were grown in medium containing "lightly" (control cells) or "heavily" (treated cells) labeled forms of the amino acids arginine and lysine. Cells were exposed to 5 μM cisplatin for 4 h, mixed with untreated cells, lysed, and subsequently digested with trypsin. The 4-h time point was selected based on the kinetics of cisplatin-induced stress responses (Fig. 1). Phosphopeptides were selectively enriched by means of a two-step phosphopeptide enrichment procedure, i.e., SCX (strong cation exchange) chromatography followed by $TiO_2$ column separation and subjected to online nanoflow liquid chromatography-tandem mass spectrometry (nano-LC-MS/MS) analysis (27). A total of 14 fractions were collected from SCX chromatography, and after $TiO_2$ enrichment, each fraction was analyzed by high-resolution tandem mass spectrometry on an LTQ-Orbitrap Velos MS (41) using higher-energy collisional dissociation (HCD) (40) for all MS/MS events (Fig. 1E). The tandem mass spectra were identified by Mascot (www.matrixscience.com), and SILAC phosphopeptide pairs were quantified using the MaxQuant software suite (8); the final data set showed 11,034 unique phosphopeptides (false discovery rate [FDR] of <1%) originating from 3,395 proteins (see Table S1 in the supplemental material). Most phosphopeptides contained only a single phosphorylation site (Fig. 1F), but multiple phosphorylation sites were detected as well. Serine, threonine, and tyrosine phosphorylation sites comprised ~86.7%, ~13%, and ~0.3% of the sites, respectively (Fig. 1G).

The quantified phosphorylation site data set revealed that approximately 4% of the phosphopeptides underwent a more than 2-fold change in phosphorylation level after exposure to cisplatin, corresponding to 183 and 194 up- and downregulated phosphopeptides, respectively. A total of 324 phosphorylation sites were 1.5- to 2-fold upregulated, while 725 phosphorylation sites were found to be 1.5- to 2-fold downregulated (Fig. 2A; see Table S1 in the supplemental material). Many of the top 50 upregulated phosphopeptides stemmed from proteins that are known to play key roles in DNA repair, chromatin remodeling, cell cycle checkpoints ($G_1$/S and $G_2$/M), and transcription (Fig. 2B). Typically, multiple individual phosphorylation sites were identified for each protein, but interestingly, 44 proteins (most of them related to DNA repair) were found to contain both upregulated phosphorylation sites and downregulated (dephosphorylated) sites (see Fig. S2 in the supplemental material).

To examine the general validity of our findings, we performed an independent experiment with the same ES cell line employing an identical concentration of cisplatin and exposure

time (4 h), as well as identical protocols to purify phosphopeptides (see Fig. S6A in the supplemental material). The final data set showed 11,966 unique phosphopeptides (see Table S6 in the supplemental material). The quantified phosphorylation site data set revealed that 224 and 706 up- and downregulated phosphopeptides, respectively, underwent more than 2-fold change in phosphorylation level after exposure to cisplatin (see Fig. S6C).

**Cellular network analysis.** Network and pathway analysis using MetaCore software indicated that processes related to DDR (i.e., cell cycle control, checkpoint activation, and apoptosis) were significantly overrepresented among proteins containing upregulated phosphorylation sites (>1.5-fold and >2-fold) (Fig. 2C to E; see Fig. S3 in the supplemental material). The central signal transducers in the early cellular response to cisplatin are the protein kinases ATM and ATR (Fig. 3A and B). On the other hand, the analysis of proteins containing downregulated phosphorylation sites identified cytoskeleton and mitotic processes (>1.5-fold and >2-fold). Anaphase-promoting complex (APC), cell adhesion, Rho GTPases (RAC1 and Cdc42), and mitosis initiation pathways were found to be significantly affected (Fig. 2D to F; see Fig. S3 in the supplemental material). Together, the strong inhibition of replicative DNA synthesis, the formation of DNA strand breaks, and the reduction of the mitotic index fit well with the activation of DDR (i.e., cell cycle checkpoints, DNA repair, and apoptosis) and inactivation of processes related to mitosis. Analysis of phosphorylation levels revealed the same processes significantly affected by cisplatin, when thresholds were set at 1.5- or 2.0-fold changes. This finding indicates that a 1.5-fold change in the phosphoprotein level is a relevant threshold to identify proteins and processes related to the genotoxic stress induced by cisplatin.

**Activation of ATM and ATR in response to cisplatin.** In line with recent investigations (2, 3, 30, 59), we found that DNA-damaging agents such as cisplatin provoke activation of ATM and ATR kinases as the substrate consensus sequence (SQ-TQ motif) of these kinases was significantly overrepresented (84 out of 183 peptide count) among the >2-fold-upregulated phosphorylation sites (Fig. 3A). Interestingly, whereas the phosphorylation of $S^{1987}$, the important SQ motif in murine ATM required for its activation (45), was found to be upregulated, phosphorylation of SQ motifs in ATR was not detected. Notably, phosphorylation at $S^{440}$ in ATR was found to be upregulated, suggesting that the activity of this kinase may also be modulated by phosphorylation at a site different from the SQ motif. Direct targets of ATR and ATM included proteins involved in the initial enzymatic processing step of DNA damage, such as DNA strand breaks (i.e., Nbs1, Rad50, and H2AX), signaling mediators (i.e., MDC1 and 53BP1), repair factors (i.e., BRCA1, BARD1, and FANCD2), and checkpoint activators (i.e., CHK1) (1). Interestingly, we identified multiple regulated phosphorylation sites on chromatin remodeling proteins (i.e., SMARCAD1, Chd1, Ino80, Rsf1, and HMGA1), E3 ubiquitin ligases (i.e., Np95, Ube3a, Huwe1, Rnf2, UBR7, Mdm2, TRIM33, and RNF19A), and a SUMO protein ligase (i.e., RanBP2). Moreover, proteins known to bind cisplatin-DNA adducts such as the high-mobility group proteins HMGA1 and HMGA2 (62), revealed altered phosphorylation site abundance after treatment. The phosphorylation of the

**A** Phosphopeptide ratio plot

Phosphosite ratio > 2 [count:183] or < 0.5 [count:194]

1.5 < Phosphosite ratio < 2 [count:324] or 0.5 < ratio < 0.67 [count:725]

0.67 < Phosphosite ratio < 1.5 [count:8205]

y axis: Phosphopeptide MS signal intensity [counts/sec]
x axis: Phosphopeptide ratio [H/L normalized]

**B**

| Gene Names | Phosphosite position | SILAC Ratio H/L |
|---|---|---|
| Brca1 | 1422 | 11,01 |
| Pctk2 | 180 | 10,15 |
| Tnk1 | 515 | 10,05 |
| Rfc5 | 7 | 9,59 |
| Tsg118 | 165 | 9,46 |
| Mdc1 | 176 | 7,88 |
| Arhgef19 | 336 | 6,89 |
| Uhrf1 | 169 | 6,87 |
| Trp53bp1 | 305 | 6,86 |
| Hmga1 | 9 | 6,77 |
| Rsf1 | 528 | 6,19 |
| Taf1c | 763 | 5,88 |
| Acin1 | 380 | 5,79 |
| Kdm4b | 453 | 5,58 |
| Brca1 | 1197 | 5,53 |
| Chek1 | 317 | 5,52 |
| Bard1 | 543 | 5,42 |
| Srrm2 | 375 | 5,39 |
| Srrm2 | 385 | 5,39 |
| Ppm1g | 201 | 5,38 |
| Mcm6 | 13 | 5,08 |
| Smtn | 798 | 4,89 |
| Impact | 9 | 4,84 |
| Hdac3 | 74 | 4,71 |
| Cggbp1 | 164 | 4,50 |
| Chd1 | 1396 | 4,45 |
| Ncapd2 | 598 | 4,28 |
| Ncapd2 | 1300 | 4,26 |
| Rad51c | 365 | 4,15 |
| Orc1l | 258 | 4,12 |
| Orc1l | 255 | 4,12 |
| Mki67 | 2185 | 4,11 |
| Wdhd1 | 898 | 4,09 |
| Ranbp3 | 283 | 4,05 |
| Ranbp3 | 277 | 4,05 |
| Pus7 | 40 | 3,98 |
| Palb2 | 154 | 3,96 |
| Nsmce4a | 375 | 3,91 |
| Pus1 | 103 | 3,90 |
| Nbn | 398 | 3,83 |
| Rps6ka6 | 510 | 3,76 |
| Psma1 | 247 | 3,75 |
| Rad50 | 690 | 3,73 |
| Ncl | 425 | 3,66 |
| Zmym4 | 1065 | 3,64 |
| Nbn | 58 | 3,59 |
| Numa1 | 270 | 3,58 |
| Hp1bp3 | 144 | 3,57 |
| Tnks1bp1 | 1611 | 3,49 |
| H2ax | 140 | 3,39 |

**C**

| Gene Names | Phosphosite position | SILAC Ratio H/L |
|---|---|---|
| Kcne4 | 69 | 0,01 |
| Golga4 | 891 | 0,01 |
| Klf3 | 91 | 0,03 |
| Bat2d1 | 1051 | 0,06 |
| Rbm20 | 1020 | 0,07 |
| Aff1 | 764 | 0,07 |
| Rbm33 | 531 | 0,09 |
| Aof2 | 167 | 0,11 |
| Rad51ap1 | 256 | 0,12 |
| Mtl5 | 178 | 0,14 |
| Sptbn1 | 2186 | 0,15 |
| Syt13 | 67 | 0,15 |
| Trappc9 | 971 | 0,16 |
| Triobp | 328 | 0,17 |
| Triobp | 324 | 0,17 |
| 8030462N17Rik | 147 | 0,17 |
| 4930594M22Rik | 5 | 0,17 |
| Pds5b | 1176 | 0,18 |
| Nbr1 | 701 | 0,19 |
| Nbr1 | 700 | 0,19 |
| Slc7a1 | 616 | 0,21 |
| Kiaa1305 | 615 | 0,21 |
| Rbm33 | 816 | 0,22 |
| Parg | 297 | 0,22 |
| Nacc1 | 145 | 0,23 |
| Kdm1 | 132 | 0,23 |
| Ythdf2 | 2 | 0,24 |
| Map7d1 | 275 | 0,24 |
| Utf1 | 99 | 0,25 |
| Map3k7ip1 | 7 | 0,25 |
| Map4 | 99 | 0,27 |
| Eif4ebp2 | 65 | 0,27 |
| Nfatc4 | 264 | 0,28 |
| Acin1 | 137 | 0,28 |
| Pcm1 | 1826 | 0,28 |
| OTTMUSG00000016543 | 70 | 0,29 |
| Rod1 | 27 | 0,29 |
| Ag2 | 210 | 0,29 |
| Atad2 | 168 | 0,29 |
| Acaca | 1296 | 0,30 |
| Acaca | 1300 | 0,30 |
| Nfatc4 | 120 | 0,31 |
| Gapvd1 | 996 | 0,31 |
| Asxl2 | 1254 | 0,31 |
| Brd8 | 175 | 0,31 |
| Arhgap11a | 946 | 0,32 |
| Nfatc4 | 217 | 0,33 |
| Nfatc4 | 213 | 0,33 |
| Esrrb | 207 | 0,33 |
| Slc1a4 | 507 | 0,33 |

**D** Process Networks (Up-regulated phosphosites) — -log(pValue)

DNA damage Checkpoint; Cell cycle G2-M; DNA damage MMR repair; Cell cycle S phase; DNA damage DBS repair; DNA damage Core; DNA damage BER-NER repair; Apoptosis Apoptotic nucleus; Cell cycle G1-S; Cell cycle Meiosis

**E** Process Networks (Down-regulated phosphosites) — -log(pValue)

Cytoskeleton Spindle microtubules; Cell cycle Mitosis; Cell adhesion Cell junctions; Cytoskeleton Actin filaments; Cytoskeleton Regulation; Cytoskeleton Cytoplasmic microtubules; Transcription Chromatin modification; Cell adhesion Cadherins; Cell cycle S phase; ESR1-nuclear pathway

**F** Process Networks (Up-regulated phosphosites) — -log(pValue)

DNA damage Checkpoint; Cell cycle G2-M; DNA damage MMR repair; DNA damage Core; Cell cycle S phase; DNA damage BER-NER repair; DNA damage DBS repair; Apoptosis Apoptotic nucleus; Cell cycle G1-S; Transcription Chromatin modification

**G** Process Networks (Down-regulated phosphosites) — -log(pValue)

Cytoskeleton Spindle microtubules; Cell cycle Core; Cell cycle Mitosis; Cytoskeleton Regulation; Cell cycle S phase; Cell cycle G1-S; Cardiac development FGF ErbB signaling; DNA damage Checkpoint; Transcription Chromatin modification; Cardiac development Wnt signaling
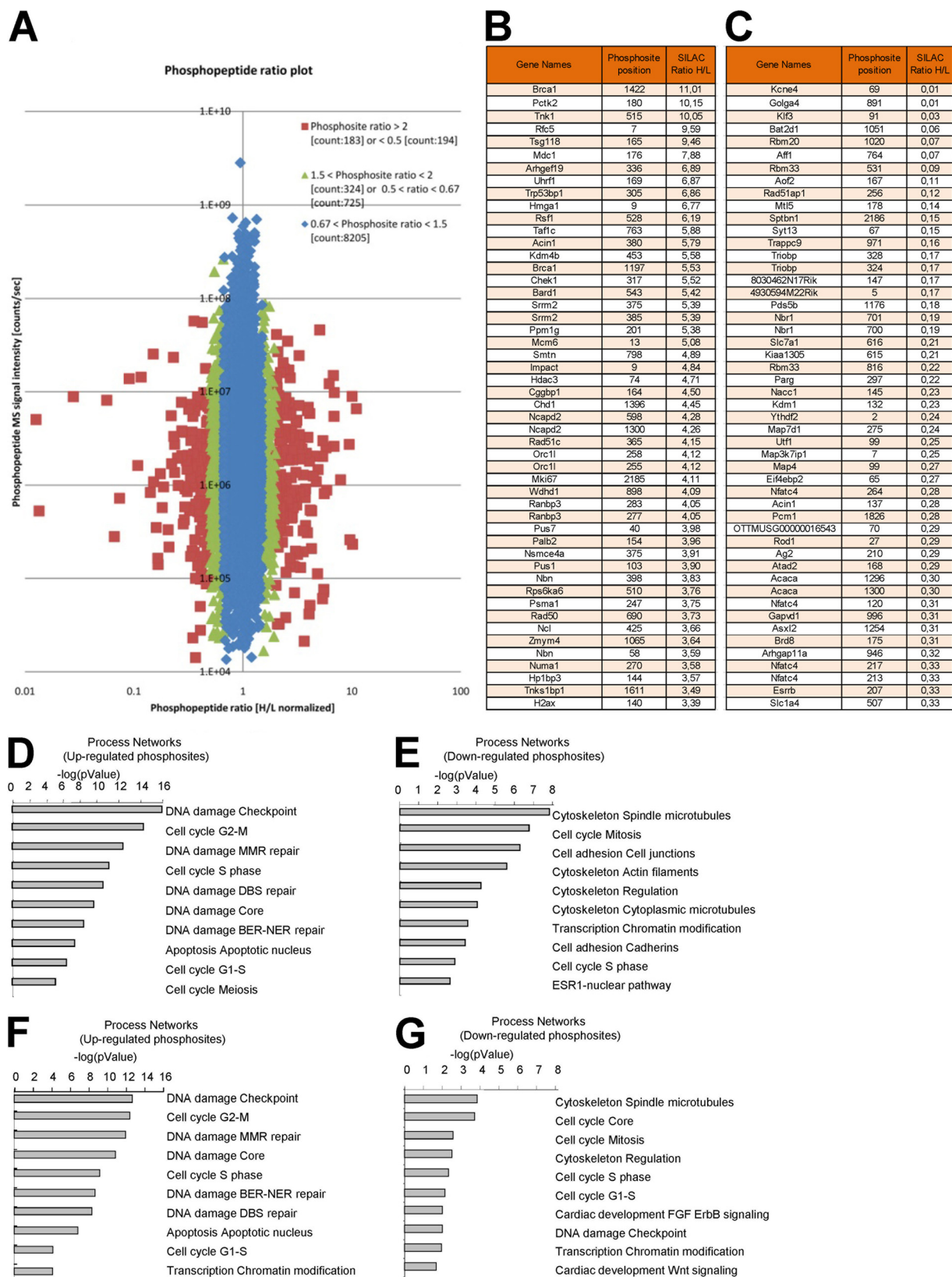
FIG. 2. (A) Phosphopeptide ratio plot. Red dots indicate phosphopeptides that were found to be >2-fold up- or downregulated after cisplatin treatment; green dots indicate phosphopeptides that showed 1.5- to 2-fold up- and downregulation after cisplatin treatment; blue dots indicate phosphopeptides that were not affected by cisplatin treatment. The y axis represents signal intensity of the ions, and it is related to the power (~amplitude squared) of the signal sine wave. (B) Top 50 upregulated phosphopeptides. (C) Top 50 downregulated phosphopeptides. (D) MetaCore network analysis of proteins containing >1.5-fold-upregulated phosphorylation sites after cisplatin treatment. (E) MetaCore network analysis of proteins containing more than 1.5-fold-downregulated phosphorylation sites after cisplatin treatment. (F) MetaCore network analysis of proteins containing >2-fold-upregulated phosphorylation sites after cisplatin treatment. (G) MetaCore network analysis of proteins containing >2-fold downregulated phosphorylation sites after cisplatin treatment.

**A**



Over-represented Kinase motifs among
the up-regulated phosphosites (Ratio > 2)

ATM/ATR/DNA-PK motif
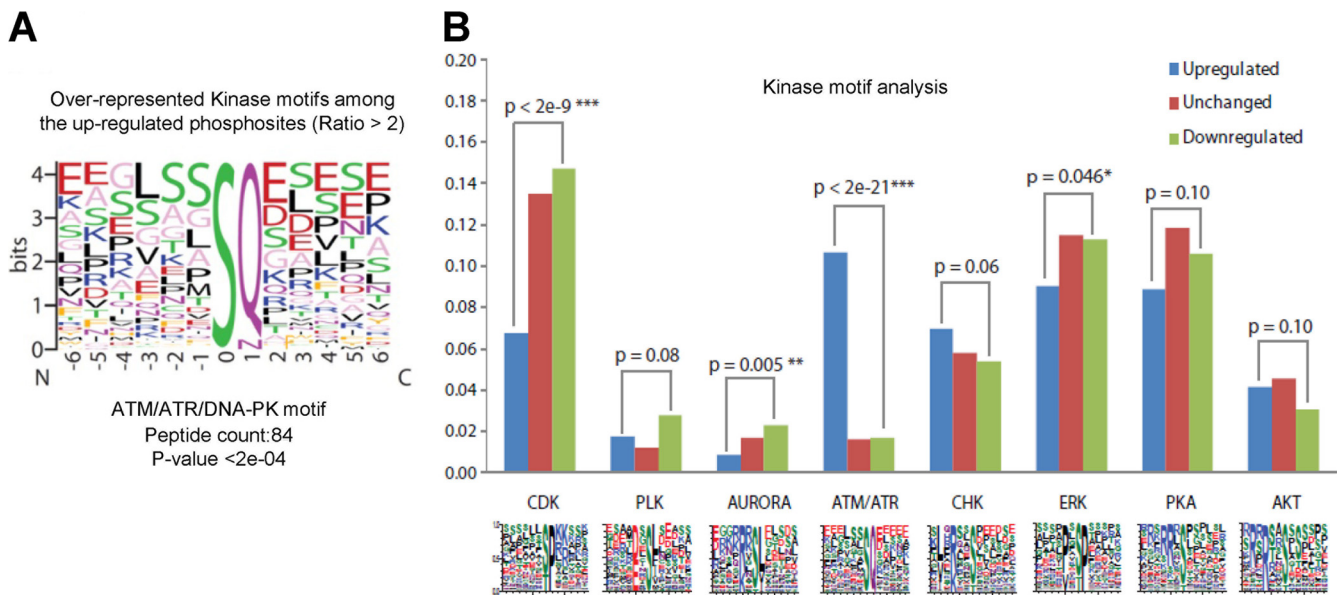Peptide count: 84
P-value <2e-04

**B**



FIG. 3. (A) Consensus sequence for ATM, ATR, and DNA-PK substrates among the >2-fold-upregulated phosphorylation sites. (B) Consensus sequence for different kinases among upregulated, downregulated, and unmodified phosphorylation sites.

acidic C-terminal tail of HMGA2 has been associated with reduced DNA binding activity (56). Phosphorylation sites $S^{100}$, $S^{101}$, and $S^{104}$ on the acidic C-terminal tail and $S^{44}$ outside that domain of HMGA2 were found to be downregulated after cisplatin treatment, suggesting increased DNA binding to cisplatin-modified DNA. In contrast, we observed enhanced phosphorylation of the $S^{102}$ and $S^{103}$ sites on the acidic C-terminal tail of HMGA1 after cisplatin treatment, and, moreover, the phospho-$S^9$ (SQ motif) was present in the top 10 cisplatin-upregulated phosphorylation sites.

**Kinase domain loop phosphorylation site changes by cisplatin stress response.** Based on the consensus sequence, about half of the >2-fold-upregulated phosphorylation sites were not canonical substrates of ATM or ATR, revealing substantial involvement of other kinases in the genotoxic stress response. The activity of many kinases is modulated by phosphorylation of the kinase domain loop located between the conserved amino acid sequence motifs DFG and APE (35). This domain plays a crucial role in substrate recognition. Phosphorylation of residues in this segment is frequently required for the correct alignment between the substrate and the catalytic site of the kinases (20), and the phosphorylation status of the activation loop can therefore be used as a proxy for kinase activity. Eleven kinases mainly belonging to the MAPK family were identified to be phosphorylated in the activation loop after cisplatin treatment (Fig. 4A). Plk1, a kinase that plays essential roles in the regulation of mitosis by coordinating spindle assembly and dynamics, was found to be specifically dephosphorylated in its activation loops after cisplatin treatment. We tested the biological relevance of 11 of the regulated kinases for cisplatin-induced toxicity by siRNA-mediated knockdown and demonstrated a novel protective role for 3 of them (CDK7, Plk1, and KPCD1) (Fig. 4B). In order to test the off-target effects, four individual siRNAs were used to knock down CDK7, Plk1, and KPCD1, respectively, and the extent of

knockdown was tested by Western blotting (see Fig. S4 in the supplemental material). We note here that a significant reduction in cell survival was detected for the Plk1 knockdown in the absence of cisplatin treatment, indicating a critical role of this kinase in normal cell growth (see Fig. S4) (65).

**Effects on mitosis.** Analysis of kinase motifs among the phosphorylation sites showed a significant enrichment of CDK, ERK, and Aurora kinase substrates among the downregulated phosphorylation sites (Fig. 3B). In response to persistent genotoxic stress, ATM and ATR and the subsequent Chk1/Chk2 signaling cascade prevent activation of Cdk1/cyclin B, thereby blocking entry into mitosis (1). The depletion of mitotic cells evidenced by FACS analysis (Fig. 1C) is consistent with the activity of these cell cycle kinases, as indicated by the phosphoproteomic data set. Following DNA damage, two mitosis-specific kinases, Cdk1 and Plk1, are inactivated by inhibitory phosphorylation ($T^{14}$ and $Y^{15}$) (36) and dephosphorylation ($T^{210}$) (64) events, respectively. $T^{14}$ and $Y^{15}$ phosphorylation of Cdk1 and the dephosphorylation of the activation loop $T^{210}$ of Plk1 were evident in our data (see Table S1 in the supplemental material). Several Plk1 targets involved in mitosis have been identified (34), including FoxM1; this protein was found to be dephosphorylated after cisplatin treatment (see Table S1). The FoxM1 protein is an important transcription factor involved in the regulation of mitotic entry (25, 71), and phosphorylation of FoxM1 by Plk1 and Cdk1 regulates the transcription network essential for mitotic progression (14). Remarkably, a wide range of proteins related to mitotic events were found to be dephosphorylated: i.e., KNSL1, nucleolin, histone H1, and the anaphase-promoting complex (APC). APC is a multisubunit protein complex with E3 ubiquitin ligase acitivity essential for proteolysis, a key mechanism that drives the events of mitosis. APC1, APC2, Cdc20, Cdh1, and Cdc23 subunits of the anaphase-promoting complex were found to be
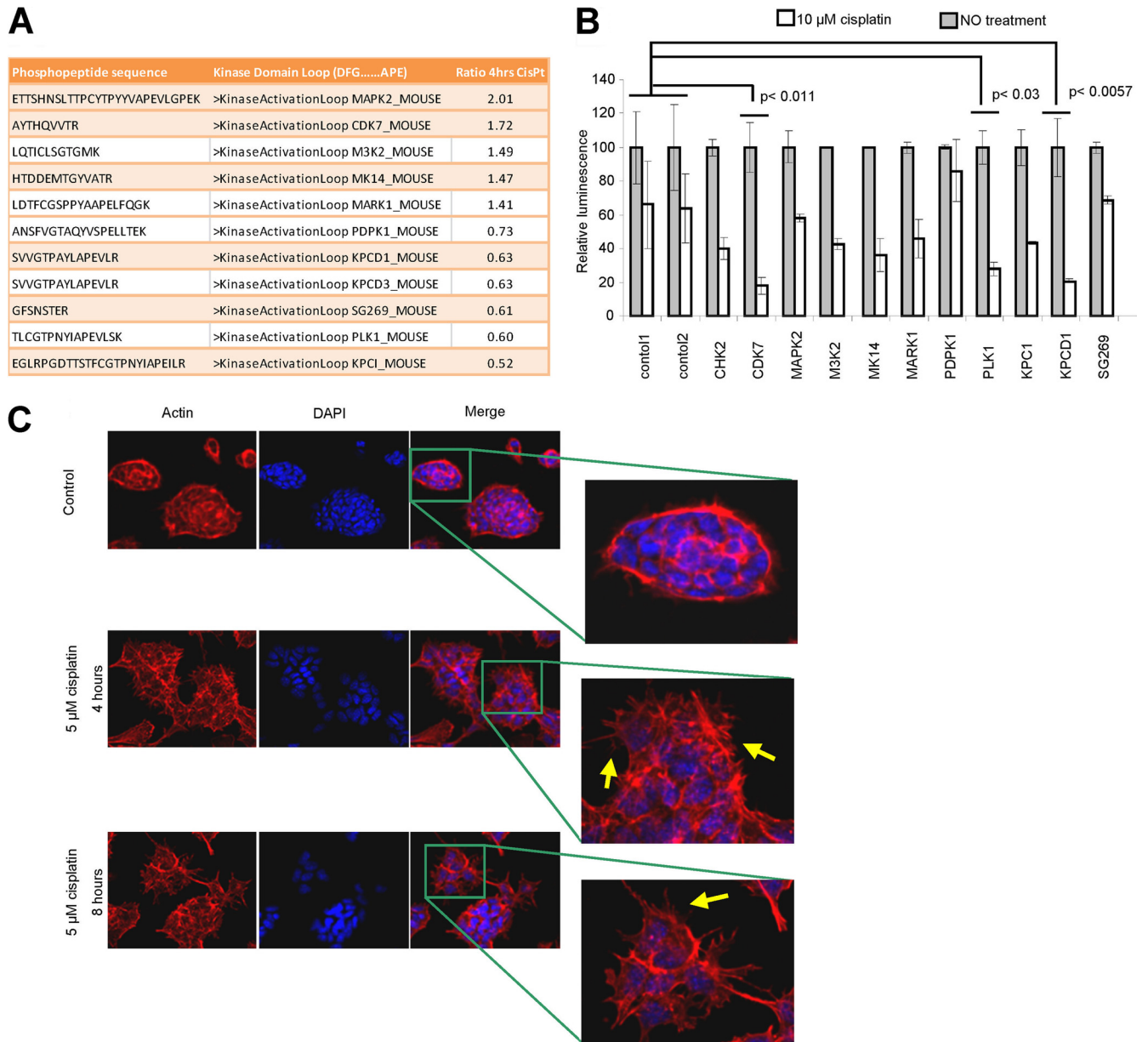
**A**

| Phosphopeptide sequence | Kinase Domain Loop (DFG......APE) | Ratio 4hrs CisPt |
|---|---|---|
| ETTSHNSLTTPCYTPYYVAPEVLGPEK | >KinaseActivationLoop MAPK2_MOUSE | 2.01 |
| AYTHQVVTR | >KinaseActivationLoop CDK7_MOUSE | 1.72 |
| LQTICLSGTGMK | >KinaseActivationLoop M3K2_MOUSE | 1.49 |
| HTDDEMTGYVATR | >KinaseActivationLoop MK14_MOUSE | 1.47 |
| LDTFCGSPPYAAPELFQGK | >KinaseActivationLoop MARK1_MOUSE | 1.41 |
| ANSFVGTAQYVSPELLTEK | >KinaseActivationLoop PDPK1_MOUSE | 0.73 |
| SVVGTPAYLAPEVLR | >KinaseActivationLoop KPCD1_MOUSE | 0.63 |
| SVVGTPAYLAPEVLR | >KinaseActivationLoop KPCD3_MOUSE | 0.63 |
| GFSNSTER | >KinaseActivationLoop SG269_MOUSE | 0.61 |
| TLCGTPNYIAPEVLSK | >KinaseActivationLoop PLK1_MOUSE | 0.60 |
| EGLRPGDTTSTFCGTPNYIAPEILR | >KinaseActivationLoop KPCI_MOUSE | 0.52 |

**B**



**C**



FIG. 4. (A) Analysis of the kinase domain loop located between the conserved sequence from DFG to APE. (B) The cellular sensitivity for cisplatin after siRNA knockdown was determined by an ATP monitoring system. Knockdown of CDK7, PLK1, or KPCD1 kinases significantly reduced cell survival after cisplatin treatment (Student's *t* test). siGFP (control 1) and siLAMIN C/A (control 2) were used as negative controls (two independent experiments). (C) Effects of cisplatin on cytoskeleton structure. mES cells were exposed for 4 and 8 h to cisplatin (5 μM) treatment and stained with DY554-phalloidin and DAPI (4′,6-diamidino-2-phenylindole) (nuclei). The arrows indicate microspikes.

down-phosphorylated, and very likely this alteration may facilitate the binding of Emi1, an inhibitor of APC (63).

**Effects on cytoskeleton.** Cellular movement is orchestrated by microtubules and actin cytoskeleton and is controlled by the activity of Rho GTPases (73). Prominent Rho GTPase family members are Rac1 and Cdc42, which induce the formation of extensions (lamellipodia) and stimulate actin polymerization at the leading edge of the cell together with the formation of new adhesion sites to the matrix (51). Cytoskeleton processes and, in particular, Rac-1 ($P < 10e-5$) and Cdc42 ($P < 10e-4$)

pathways were found to be affected by genotoxic stress (see Fig. S3 in the supplemental material). Proteins associated with the RAC-1 and Cdc42 pathways (i.e., ABR, ECT2, DBL, RacGAP1, p200RhoGAP, ARCGAP22, and ARHGAP12) were found to be dephosphorylated on proline-directed serine/threonine sites (potential CDK or MAPK substrates) or sites that are targeted by casein kinases (in an acidic amino acid context). To study the effect of cisplatin on cytoskeleton structure, we monitored the actin organization in mES cells after treatment (Fig. 4C). Cytoskeleton remodeling and specific micro-

spike formation were clearly visible in cells treated with cisplatin, confirming the results of the pathway analysis obtained from the phosphoproteome.

**Proteome and transcriptome.** Nonphosphorylated peptides were analyzed to rule out that changes in overall protein levels might be responsible for the observed changes in phosphorylation site levels. Quantitative profiles were obtained for 4,349 proteins (Fig. 5A) out of a total of 5,917 proteins (see Table S2 in the supplemental material), based on the quantification of 16,305 nonphosphorylated unique peptides (see Table S3 in the supplemental material). The abundance of most proteins that contained up- or downregulated phosphorylation sites did not change significantly during cisplatin treatment, indicating that the majority of observed phosphorylation changes were not due to alterations in protein quantity (Fig. 5C to E). Interestingly, cellular levels of 455 proteins were found to be altered when proteomic data analysis was performed with a statistical rigor of $P < 0.05$. Network analysis identified cytoskeleton remodeling as one of the most prominent affected pathways. In particular, the NOTCH signaling pathway was statistically found to be significantly affected (see Fig. S3 in the supplemental material). MetaCore analysis shows an enrichment of p53 target genes (i.e., 49 out of 455 proteins) double the expected frequency ($P < 10e-6$), suggesting a p53-dependent response, in line with previous studies (24). We examined how the proteome correlates to the mES transcriptome previously generated under identical conditions of cell growth and cisplatin exposure (24). Of a total of 3,616 Entrez gene identifications (IDs) shared among the gene expression and protein data sets, 386 proteins and 56 mRNAs transcripts were found to be significantly affected by cisplatin treatment ($P < 0.05$), with surprisingly only 5 gene IDs being in common (see Table S5 in the supplemental material). A selected group of genes was examined by RT-PCR and Western blot analysis to quantify gene expression and protein levels in mES cells after cisplatin treatment. Indeed, significant changes in protein levels were found for Cdh1, p53, Centrin2, and Mark2 by immunoblotting, whereas the corresponding mRNA transcripts were not affected after cisplatin treatment (see Fig. S5 in the supplemental material). Together, these data indicate that alterations in protein and transcript quantities do not correlate well at the individual gene level after cisplatin treatment. In contrast, pathway analysis based on transcriptomic, proteomic, and phosphoproteomic data revealed a large overlap in the affected processes (Fig. 6). The cell cycle was the most prominent pathway affected at the transcriptome and phosphoproteome level, whereas DNA repair pathways were only significantly affected at the phosphoproteome level. In contrast, changes at the overall protein level primarily involved processes associated with cytoskeleton regulation.

## DISCUSSION

Cisplatin is a widely used anticancer drug, and, therefore, understanding of the molecular changes that underlie the biological consequences of treatment with this drug is of critical importance. Protein phosphorylation is one of the most prominent posttranslational modifications that are triggered by cisplatin treatment, and, therefore, global phosphoproteome analysis is an excellently suited approach to identify molecular components and cellular pathways affected by cisplatin.

Inhibition of transcription and replication by cisplatin-induced DNA lesions, and subsequently the generation of DNA strand breaks, activates the ATR and ATM kinases as well as p38 MAPK/MK2 pathway (1, 49, 50). Consistently, we found upregulation of $S^{1987}$ phosphorylation in ATM that is required for its activation (45). Upregulation of ATR phosphorylation was observed at $S^{440}$, a site that lacks the SQ motif and likely represents the site targeted by the NEK6 kinase. This kinase belongs to a large family of Ser/Thr kinases that have critical roles in coordinating microtubule dynamics during mitotic progression (46). This phosphorylation site has not been previously mapped and might represent a novel site involved in ATR activation. The top 50 upregulated phosphorylation sites include a significant number of direct ATR and ATM targets related to DDR—most notably proteins involved in the processing step of double-strand breaks (DSB), DNA damage signaling, stalled replication/transcription forks, checkpoint activation, and chromatin remodeling proteins. In addition, E3 ubiquitin and SUMO-protein ligases were observed to be regulated by phosphorylation events highlighting the cross talk between phosphorylation and other posttranslational modifications in response to genotoxic stress (2). In contrast to the large-scale proteomic analysis of SQ-specific phosphorylation sites in response to DNA damage induced by ionizing radiation (IR) and UV (30, 59), our global phosphoproteomic strategy allowed identification of putative ATM/ATR-dependent and -independent phosphorylation events. Indeed, DNA repair proteins such as BRCA1, Rad50, p53BP1, FANCI, and BARD-1 were found to contain upregulated phosphorylation sites unrelated to ATM and ATR activity. As these data are not based on direct experimental evidence, we cannot exclude that ATM/ATR may also phosphorylate at nonconsensus sites. Moreover, 44 proteins (mostly involved in DNA repair and including BRCA1 and Ino80; see Fig. S2 in the supplemental material) underwent differential phosphorylation of adjacent sites (2 to 5 amino acids). Differential phosphorylation might serve to create a molecular switching mechanism (2) by a tightly controlled activity of several kinases and phosphatases. Different types of posttranslational modifications controlled by such a mechanism might dynamically regulate the DDR—for example, the assembly and disassembly of factors at sites of damage (1).

Several of the HMG domain proteins recognize cisplatin adducts and display a selective affinity for clinically effective platinum drugs (22). HMGA proteins are expressed at a high levels during embryonic development, whereas they are barely detectable in differentiated or nonproliferating cells; it is noteworthy that these proteins are highly reexpressed following neoplastic transformation (57). HMGA1 and HMGA2 were found to be differentially phospho-regulated after cisplatin treatment. To our knowledge, these are the first *in vivo* data showing a discrepancy in phosphorylation states between HMGA1 and HMGA2 in response to genotoxic stress. The finding of differential phosphorylation profiles within the HMGA family after cisplatin treatment might offer potential targets for improved cisplatin cancer therapy, considering that these proteins are overexpressed in cancers of different origins.
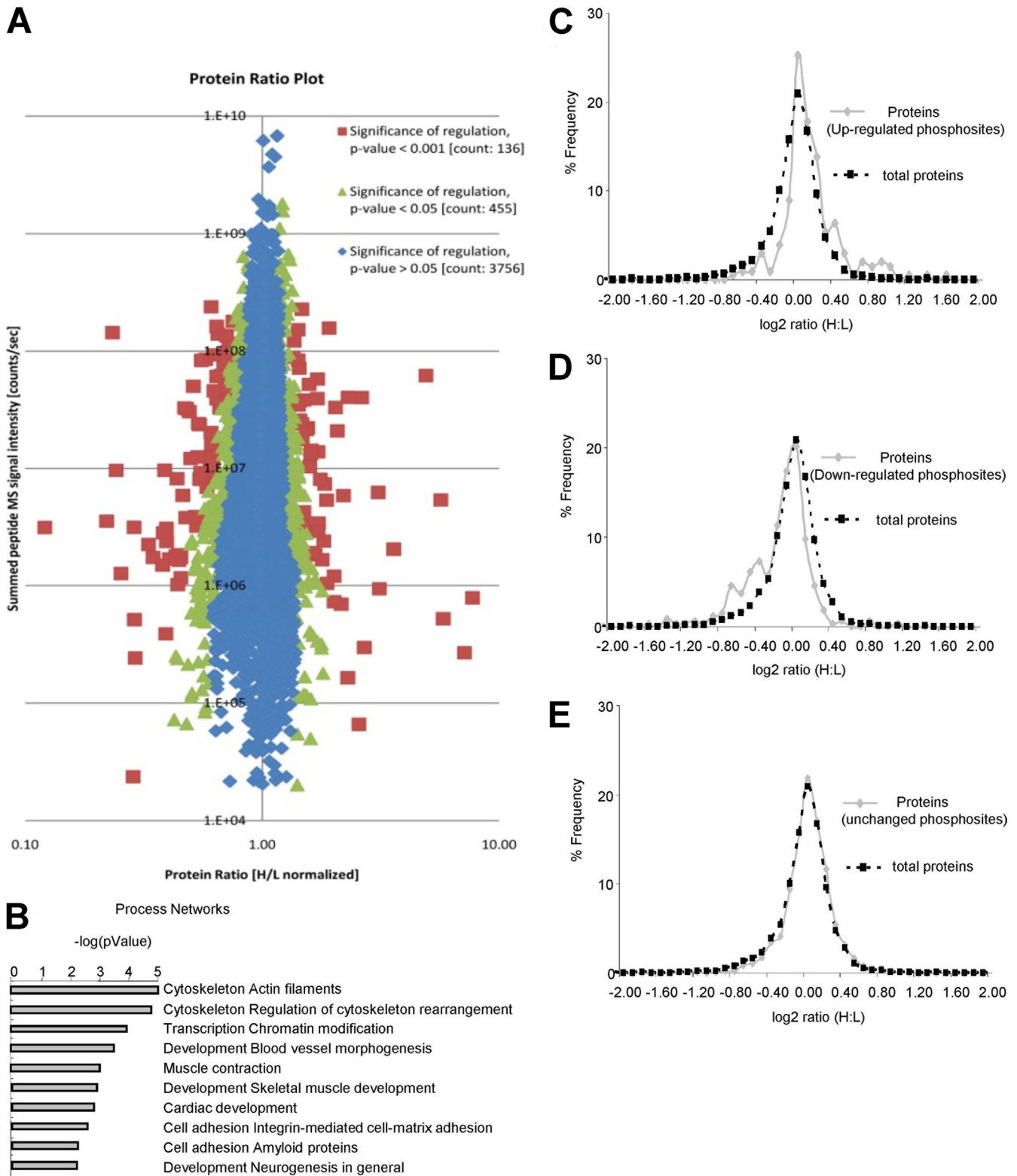
FIG. 5. (A) Unmodified peptide ratio plot. Red dots, significantly ($P < 0.001$) regulated peptides after cisplatin treatment; green dots, significantly ($P < 0.05$) regulated peptides after cisplatin treatment; blue dots, unmodified peptides after cisplatin treatment. The $y$ axis represents signal intensity of the ions and is related to the power (~amplitude squared) of the signal sine wave. (B) MetaCore network analysis of significantly affected proteins ($P < 0.05$) after cisplatin addition. (C) Abundance distributions of all proteins and proteins containing upregulated phosphorylation sites (>1.5-fold) (D) Abundance distributions of all proteins and proteins containing downregulated phosphorylation sites (>1.5-fold). (E) Abundance distributions of all proteins and proteins containing unmodified phosphorylation sites.
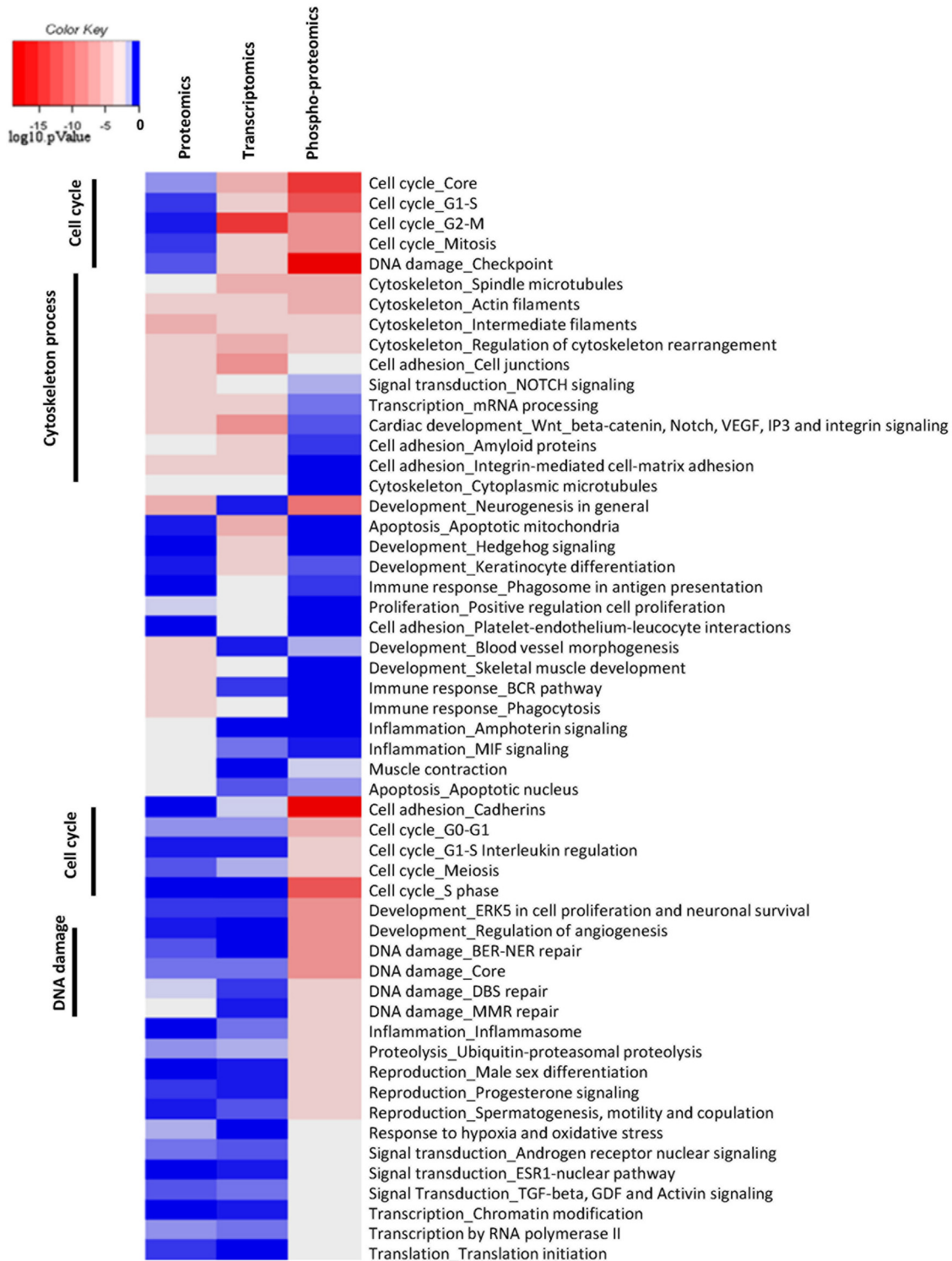
FIG. 6. Comparison of significantly affected pathways (MetaCore network analysis) by cisplatin at the transcriptomic (mRNA transcripts; $P <$ 0.05), proteomic (proteins; $P < 0.05$) and phosphoproteomic (phosphoprotein; $P < 0.05$) levels.

The outcome of an independent replicate experiment with the same ES cells demonstrated the high reproducibility of the cisplatin-induced protein phosphorylation. The results also showed that ATM and ATR consensus sequences were significantly overrepresented among hyperphosphorylated peptides (see Fig. S6D in the supplemental material). The phosphopeptide ratio correlation between the two replicates is 0.61 (Pearson correlation coefficient, $R$; see Fig. S6A) based on 7,275

unique phosphopeptides identified in both experiments (see Table S7 in the supplemental material). These results are close to those achieved in a recent study using a similar experimental approach (52). A much higher correlation ($R = 0.88$) was found when the analysis was limited to putative ATM/ATR substrate peptide ratios (see Fig. S6A, B, and E). Importantly, network analysis identified DDR and cytoskeleton regulation as affected cisplatin processes in both experiments. Together these results demonstrate the reproducibility and general validity of our findings (see Fig. S6F and G).

Our results indicate that the cellular response to genotoxic stress involves a large variety of protein kinases and phosphatases. Indeed, 11 kinases were identified to be regulated at phosphorylation sites in the activation loop after cisplatin treatment (Fig. 4A). Most of those regulated belong to the MAPK family, but a kinase not related to the MAPK family (i.e., Plk1 essential in the regulation of mitosis) was found to be dephosphorylated as well. Mitogen-activated protein kinases (MAPKs) are critical components of the signaling network activated by genotoxic stress and are critical in deciding cell fate in response to cisplatin (5). Particularly, in the absence of p53, cells depend on p38 MAPK/MK2 for cell cycle arrest and survival after cisplatin (49). Here we show that the kinase domain of MK14 (p38$\alpha$) is activated by specific phosphorylation of the activation loop TXY motif after cisplatin addition.

Knockdown of CDK7 significantly increased cell toxicity after cisplatin treatment. The cyclin-dependent protein kinase CDK7 forms a trimeric complex with cyclin H and MAT1 and is both a Cdk-activating kinase (CAK) (10, 48) and an essential component of the transcription factor TFIIH, involved in transcription initiation and nucleotide excision repair (55). In addition, knockdown of Plk1 and KPCD1 also increased cisplatin-mediated cytotoxicity (Fig. 4B). KPCD1 is a member of the protein kinase C (PKC) family involved in extracellular receptor-mediated signal transduction pathways (19). The mitosis-specific kinase Plk1 has been shown to play an essential role in the regulation of mitotic progression, including mitotic entry, spindle formation, chromosome segregation, and cytokinesis; moreover, it has been found to be overexpressed in different types of tumors (60). Inhibition of Plk1 is an efficient way to establish an irreversible $G_2$ arrest after DNA damage induction in specific cancers with nonfunctional p53. In these cells, typical $G_1$ arrest is lost in response to DNA damage and cells display a stronger dependence on the $G_2$ DNA damage checkpoint for protection against genotoxic insults (67) Our data suggest that the cellular response to inactivate PKL1 is directed toward prevention of mitotic entry in favor of an apoptosis process (28), which is in accordance with transcriptomic and phosphoproteomic analyses. Currently, several Plk inhibitors are in phase I or II clinical studies (9, 18, 33), and in cancers with nonfunctional p53, Plk1 inhibition serves as a potent adjuvant therapy when combined with a DNA-damaging regimen such as cisplatin (65). Together, our results clearly indicate that dissection of the cellular responses induced by cisplatin using phosphoproteome analysis in concert with functional genomics allows unraveling of targets and pathways that enhance the cytotoxic effects of cisplatin.

Proteins that were identified to be differentially phosphorylated upon cisplatin treatment also belonged to biological processes and structures not classified as or related to core DDR processes. In fact, unanticipated processes associated with cytoskeleton events were identified by network analysis of proteins containing downregulated phosphorylation sites, and in particular, Rac-1 and Cdc42 pathways were found to be affected by cisplatin. The actin component of the cytoskeleton is dynamically implicated in a variety of cell functions, including regulation of cell shape, adhesion, and motility, and recent studies underline mechanisms of cisplatin-mediated inhibition on invasion and migration of human cancer cells (21, 44, 47). Cytoskeleton remodeling and specifically the induction of microspike formation were clear effects of cisplatin treatment (Fig. 4C). These results are in line with reports on microspike formation related to Cdc42 (66). The regulation of the phospho state of Rho GTPases (members of the Rac-1 and Cdc42 pathways) shown in this study is consistent with the observed cisplatin-mediated changes in cell morphology. Moreover, the link between cisplatin and Rac-1/Cdc42 pathways is relevant in view of the fact that Cdc42 activity is associated with genome maintenance, cellular senescence regulation, and aging (72). Although classically regarded as a nuclear DNA-damaging agent, recent studies support a more promiscuous mode of action for cisplatin (12, 29, 54, 75). The current phosphoproteome analysis of kinase targets and their predicted activated substrates supports this finding by confirming previous data and providing evidence for the extranuclear targeting function that might play a role in cisplatin-induced toxicity and in cell motility. A better understanding of the mechanisms of cisplatin action may provide novel therapeutic strategies that would block metastatic progression and reducing dissemination of tumor cells.

We tested the hypothesis whether changes in transcription profiling after cisplatin correlate with changes observed at the protein level. Consistent with previously published data (42), we found no clear correlation between changes in the relative levels of transcripts and corresponding proteins. This lack of correlation might be due to the fact that the cellular mechanisms involved in regulation of stability/degradation differ between mRNAs and their encoded proteins. This finding indicates that the pieces of information derived from transcriptomic and proteomic analyses are different, but when merged generate a more comprehensive view of the signaling pathways affected by stressors. Interestingly, the phosphoproteomic analysis performed in our study led to the identification of most of the pathways that were affected at the transcriptome or proteome level. However, the impact of cisplatin on the DNA damage repair pathways was only manifested in the phosphoproteome analysis, indicating that phosphorylation events are key to activate DNA repair pathways after genotoxic stress induced by cisplatin or in general to genotoxic agents that induce replication and transcription blocking lesions.

## ACKNOWLEDGMENTS

## REFERENCES

1. **Bartek, J., and J. Lukas.** 2007. DNA damage checkpoints: from initiation to recovery or adaptation. Curr. Opin. Cell Biol. **19:**238–245.
2. **Bennetzen, M. V., et al.** 2010. Site-specific phosphorylation dynamics of the nuclear proteome during the DNA damage response. Mol. Cell Proteomics **9:**1314–1323.
3. **Bensimon, A., et al.** 2010. ATM-dependent and -independent dynamics of the nuclear phosphoproteome after DNA damage. Sci. Signal. **3:**rs3.
4. **Borst, P., S. Rottenberg, and J. Jonkers.** 2008. How do real tumors become resistant to cisplatin? Cell Cycle **7:**1353–1359.
5. **Brozovic, A., and M. Osmak.** 2007. Activation of mitogen-activated protein kinases by cisplatin and their role in cisplatin-resistance. Cancer Lett. **251:**1–16.
6. **Choudhary, C., and M. Mann.** 2010. Decoding signalling networks by mass spectrometry-based proteomics. Nat. Rev. Mol. Cell Biol. **11:**427–439.
7. **Cox, J., and M. Mann.** 2008. MaxQuant enables high peptide identification rates, individualized p.p.b.-range mass accuracies and proteome-wide protein quantification. Nat. Biotechnol. **26:**1367–1372.
8. **Cox, J., et al.** 2009. A practical guide to the MaxQuant computational platform for SILAC-based quantitative proteomics. Nat. Protoc. **4:**698–705.
9. **Degenhardt, Y., and T. Lampkin.** 2010. Targeting Polo-like kinase in cancer therapy. Clin. Cancer Res. **16:**384–389.
10. **Drapkin, R., G. Le Roy, H. Cho, S. Akoulitchev, and D. Reinberg.** 1996. Human cyclin-dependent kinase-activating kinase exists in three distinct complexes. Proc. Natl. Acad. Sci. U. S. A. **93:**6488–6493.
11. **Dronkert, M. L., and R. Kanaar.** 2001. Repair of DNA interstrand cross-links. Mutat. Res. **486:**217–247.
12. **Emert-Sedlak, L., et al.** 2005. Involvement of cathepsin D in chemotherapy-induced cytochrome c release, caspase activation, and cell death. Mol. Cancer Ther. **4:**733–742.
13. **Fousteri, M., W. Vermeulen, A. A. van Zeeland, and L. H. Mullenders.** 2006. Cockayne syndrome A and B proteins differentially regulate recruitment of chromatin remodeling and repair factors to stalled RNA polymerase II in vivo. Mol. Cell **23:**471–482.
14. **Fu, Z., et al.** 2008. Plk1-dependent phosphorylation of FoxM1 regulates a transcriptional programme required for mitotic progression. Nat. Cell Biol. **10:**1076–1082.
15. **Furuta, T., et al.** 2002. Transcription-coupled nucleotide excision repair as a determinant of cisplatin sensitivity of human cells. Cancer Res. **62:**4899–4902.
16. **Hall, M. D., M. Okabe, D. W. Shen, X. J. Liang, and M. M. Gottesman.** 2008. The role of cellular accumulation in determining sensitivity to platinum-based chemotherapy. Annu. Rev. Pharmacol. Toxicol. **48:**495–535.
17. **Jackson, S. P., and J. Bartek.** 2009. The DNA-damage response in human biology and disease. Nature **461:**1071–1078.
18. **Jimeno, A., et al.** 2010. A fine-needle aspirate-based vulnerability assay identifies polo-like kinase 1 as a mediator of gemcitabine resistance in pancreatic cancer. Mol. Cancer Ther. **9:**311–318.
19. **Johannes, F. J., J. Prestle, S. Eis, P. Oberhagemann, and K. Pfizenmaier.** 1994. PKCu is a novel, atypical member of the protein kinase C family. J. Biol. Chem. **269:**6140–6148.
20. **Johnson, L. N., M. E. Noble, and D. J. Owen.** 1996. Active and inactive protein kinases: structural basis for regulation. Cell **85:**149–158.
21. **Karam, A. K., et al.** 2010. Cisplatin and PI3kinase inhibition decrease invasion and migration of human ovarian carcinoma cells and regulate matrix-metalloproteinase expression. Cytoskeleton (Hoboken) **67:**535–544.
22. **Kartalou, M., and J. M. Essigmann.** 2001. Recognition of cisplatin adducts by cellular proteins. Mutat. Res. **478:**1–21.
23. **Keys, H. M., et al.** 1999. Cisplatin, radiation, and adjuvant hysterectomy compared with radiation and adjuvant hysterectomy for bulky stage IB cervical carcinoma. N. Engl. J. Med. **340:**1154–1161.
24. **Kruse, J. J., et al.** 2007. A portrait of cisplatin-induced transcriptional changes in mouse embryonic stem cells reveals a dominant p53-like response. Mutat. Res. **617:**58–70.
25. **Laoukili, J., et al.** 2005. FoxM1 is required for execution of the mitotic programme and chromosome stability. Nat. Cell Biol. **7:**126–136.
26. **Loehrer, P. J., and L. H. Einhorn.** 1984. Drugs five years later. Cisplatin. Ann. Intern. Med. **100:**704–713.
27. **Macek, B., M. Mann, and J. V. Olsen.** 2009. Global and site-specific quantitative phosphoproteomics: principles and applications. Annu. Rev. Pharmacol. Toxicol. **49:**199–221.
28. **Macurek, L., et al.** 2008. Polo-like kinase-1 is activated by aurora A to promote checkpoint recovery. Nature **455:**119–123.
29. **Mandic, A., J. Hansson, S. Linder, and M. C. Shoshan.** 2003. Cisplatin induces endoplasmic reticulum stress and nucleus-independent apoptotic signaling. J. Biol. Chem. **278:**9100–9106.
30. **Matsuoka, S., et al.** 2007. ATM and ATR substrate analysis reveals extensive protein networks responsive to DNA damage. Science **316:**1160–1166.
31. **McWhinney, S. R., R. M. Goldberg, and H. L. McLeod.** 2009. Platinum neurotoxicity pharmacogenetics. Mol. Cancer Ther. **8:**10–16.
32. **Morris, M., et al.** 1999. Pelvic radiation with concurrent chemotherapy compared with pelvic and para-aortic radiation for high-risk cervical cancer. N. Engl. J. Med. **340:**1137–1143.
33. **Mross, K., et al.** 2008. Phase I dose escalation and pharmacokinetic study of BI 2536, a novel Polo-like kinase 1 inhibitor, in patients with advanced solid tumors. J. Clin. Oncol. **26:**5511–5517.
34. **Nigg, E. A.** 2001. Mitotic kinases as regulators of cell division and its checkpoints. Nat. Rev. Mol. Cell Biol. **2:**21–32.
35. **Nolen, B., S. Taylor, and G. Ghosh.** 2004. Regulation of protein kinases; controlling activity through activation segment conformation. Mol. Cell **15:**661–675.
36. **O'Farrell, P. H.** 2001. Triggering the all-or-nothing switch into mitosis. Trends Cell Biol. **11:**512–519.
37. **Oliver, T. G., et al.** 2010. Chronic cisplatin treatment promotes enhanced damage repair and tumor progression in a mouse model of lung cancer. Genes Dev. **24:**837–852.
38. **Olsen, J. V., et al.** 2006. Global, in vivo, and site-specific phosphorylation dynamics in signaling networks. Cell **127:**635–648.
39. **Olsen, J. V., et al.** 2005. Parts per million mass accuracy on an Orbitrap mass spectrometer via lock mass injection into a C-trap. Mol. Cell Proteomics **4:**2010–2021.
40. **Olsen, J. V., et al.** 2007. Higher-energy C-trap dissociation for peptide modification analysis. Nat. Methods **4:**709–712.
41. **Olsen, J. V., et al.** 2009. A dual pressure linear ion trap Orbitrap instrument with very high sequencing speed. Mol. Cell Proteomics **8:**2759–2769.
42. **Olsen, J. V., et al.** 2010. Quantitative phosphoproteomics reveals widespread full phosphorylation site occupancy during mitosis. Sci. Signal. **3:**ra3.
43. **Ong, S. E., et al.** 2002. Stable isotope labeling by amino acids in cell culture, SILAC, as a simple and accurate approach to expression proteomics. Mol. Cell Proteomics **1:**376–386.
44. **Paduch, R., W. Rzeski, and J. Klatka.** 2009. The effect of cisplatin on human larynx carcinoma cell motility. Folia Histochem. Cytobiol. **47:**75–79.
45. **Pellegrini, M., et al.** 2006. Autophosphorylation at serine 1987 is dispensable for murine Atm activation in vivo. Nature **443:**222–225.
46. **Quarmby, L. M., and M. R. Mahjoub.** 2005. Caught Nek-ing: cilia and centrioles. J. Cell Sci. **118:**5161–5169.
47. **Ramer, R., K. Eichele, and B. Hinz.** 2007. Upregulation of tissue inhibitor of matrix metalloproteinases-1 confers the anti-invasive action of cisplatin on human cancer cells. Oncogene **26:**5822–5827.
48. **Reardon, J. T., et al.** 1996. Isolation and characterization of two human transcription factor IIH (TFIIH)-related complexes: ERCC2/CAK and TFIIH. Proc. Natl. Acad. Sci. U. S. A. **93:**6482–6487.
49. **Reinhardt, H. C., A. S. Aslanian, J. A. Lees, and M. B. Yaffe.** 2007. p53-deficient cells rely on ATM- and ATR-mediated checkpoint signaling through the p38MAPK/MK2 pathway for survival after DNA damage. Cancer Cell **11:**175–189.
50. **Reinhardt, H. C., and M. B. Yaffe.** 2009. Kinases that control the cell cycle in response to DNA damage: Chk1, Chk2, and MK2. Curr. Opin. Cell Biol. **21:**245–255.
51. **Ridley, A. J.** 2001. Rho GTPases and cell migration. J. Cell Sci. **114:**2713–2722.
52. **Rigbolt, K. T., et al.** 2011. System-wide temporal characterization of the proteome and phosphoproteome of human embryonic stem cell differentiation. Sci. Signal. **4:**rs3.
53. **Safaei, R., and S. B. Howell.** 2005. Copper transporters regulate the cellular pharmacology and sensitivity to Pt drugs. Crit. Rev. Oncol. Hematol. **53:**13–23.
54. **Safaei, R., et al.** 2005. Intracellular localization and trafficking of fluorescein-labeled cisplatin in human ovarian carcinoma cells. Clin. Cancer Res. **11:**756–767.
55. **Scrace, S. F., et al.** 2008. Transient treatment with CDK inhibitors eliminates proliferative potential even when their abilities to evoke apoptosis and DNA damage are blocked. Cell Cycle **7:**3898–3907.
56. **Sgarra, R., et al.** 2009. Macroscopic differences in HMGA oncoproteins post-translational modifications: C-terminal phosphorylation of HMGA2 affects its DNA binding properties. J. Proteome Res. **8:**2978–2989.
57. **Sgarra, R., et al.** 2004. Nuclear phosphoproteins HMGA and their relationship with chromatin structure and cancer. FEBS Lett. **574:**1–8.
58. **Soufi, B., et al.** 2009. Global analysis of the yeast osmotic stress response by quantitative proteomics. Mol. Biosyst. **5:**1337–1346.
59. **Stokes, M. P., et al.** 2007. Profiling of UV-induced ATM/ATR signaling pathways. Proc. Natl. Acad. Sci. U. S. A. **104:**19855–19860.
60. **Takai, N., R. Hamanaka, J. Yoshimatsu, and I. Miyakawa.** 2005. Polo-like kinases (Plks) and cancer. Oncogene **24:**287–291.
61. **Tichy, E. D., and P. J. Stambrook.** 2008. DNA repair in murine embryonic stem cells and differentiated cells. Exp. Cell Res. **314:**1929–1936.
62. **Todd, R. C., and S. J. Lippard.** 2009. Inhibition of transcription by platinum antitumor compounds. Metallomics **1:**280–291.
63. **Torres, J. Z., K. H. Ban, and P. K. Jackson.** 2010. A specific form of phospho protein phosphatase 2 regulates anaphase-promoting complex/cyclosome association with spindle poles. Mol. Biol. Cell **21:**897–904.
64. **Tsvetkov, L., and D. F. Stern.** 2005. Phosphorylation of Plk1 at S137 and T210 is inhibited in response to DNA damage. Cell Cycle **4:**166–171.
65. **Tyagi, S., et al.** 2010. Polo-like kinase1 (Plk1) knockdown enhances cisplatin

chemosensitivity via up-regulation of p73alpha in p53 mutant human epidermoid squamous carcinoma cells. Biochem. Pharmacol. **80:**1326–1334.

66. **Umikawa, M., et al.** 1999. Association of frabin with the actin cytoskeleton is essential for microspike formation through activation of Cdc42 small G protein. J. Biol. Chem. **274:**25197–25200.

67. **van Vugt, M. A., A. Bras, and R. H. Medema.** 2005. Restarting the cell cycle when the checkpoint comes to a halt. Cancer Res. **65:**7037–7040.

68. **Villen, J., S. A. Beausoleil, S. A. Gerber, and S. P. Gygi.** 2007. Large-scale phosphorylation analysis of mouse liver. Proc. Natl. Acad. Sci. U. S. A. **104:**1488–1493.

69. **Wang, D., R. Hara, G. Singh, A. Sancar, and S. J. Lippard.** 2003. Nucleotide excision repair from site-specifically platinum-modified nucleosomes. Biochemistry **42:**6747–6753.

70. **Wang, D., and S. J. Lippard.** 2005. Cellular processing of platinum anticancer drugs. Nat. Rev. Drug Discov. **4:**307–320.

71. **Wang, I. C., et al.** 2005. Forkhead box M1 regulates the transcriptional network of genes essential for mitotic progression and genes encoding the SCF (Skp2-Cks1) ubiquitin ligase. Mol. Cell. Biol. **25:**10875–10894.

72. **Wang, L., L. Yang, M. Debidda, D. Witte, and Y. Zheng.** 2007. Cdc42 GTPase-activating protein deficiency promotes genomic instability and premature aging-like phenotypes. Proc. Natl. Acad. Sci. U. S. A. **104:**1248–1253.

73. **Waterman-Storer, C. M., and E. Salmon.** 1999. Positive feedback interactions between microtubule and actin dynamics during cell motility. Curr. Opin. Cell Biol. **11:**61–67.

74. **Welsh, C., et al.** 2004. Reduced levels of XPA, ERCC1 and XPF DNA repair proteins in testis tumor cell lines. Int. J. Cancer **110:**352–361.

75. **Zeidan, Y. H., R. W. Jenkins, and Y. A. Hannun.** 2008. Remodeling of cellular cytoskeleton by the acid sphingomyelinase/ceramide pathway. J. Cell Biol. **181:**335–350.